Electronic Supplementary Material (ESI) for Lab on a Chip.
This journal is © The Royal Society of Chemistry 2017

Supplementary information *for*

Subnanometer structure and function from ion beams through complex fluidics to fluorescent particles

Kuo-Tang Liao,[ab] Joshua Schumacher,[a] Henri J. Lezec[a] and Samuel M. Stavis*[a]

Index

Fig. S1 Atomic reference material

Fig. S2 Roughness uncertainty

Fig. S3 Rapid prototyping

Table S1 Patterning variables

Fig. S4 Beam overlapping

Fig. S5 Aliasing artifact

Fig. S6 Lateral resolution

Fig. S7 Pattern integration

Table S2 Ion penetration

Fig. S8 Test pattern

Table S3 Fig. 3 analysis

Fig. S9 Milling silicon

Fig. S10 Structural colors

Video S1 Nanoparticle separation

Fig. S11 Analytical separation

Fig. S12 Emission spectra

Fig. S13 Dye loading

Fig. S14 Photobleaching analysis

Fig. S15 Device layout

Note S1 Interference calibration

Supplementary references

[a] *Center for Nanoscale Science and Technology, National Institute of Standards and Technology, Gaithersburg, Maryland 20899, USA.*

E-mail: samuel.stavis@nist.gov

[b] *Maryland Nanocenter, University of Maryland, College Park, Maryland 20742, USA*

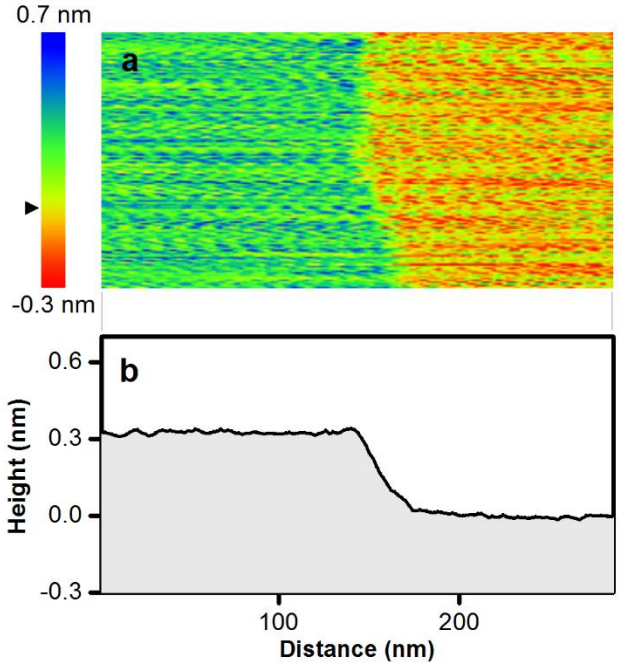

Fig. S1 Atomic reference material. Highly ordered pyrolytic graphite has a monolayer thickness with a nominal value of 0.335 nm.[1] (a) Representative atomic force micrograph and (b) corresponding section showing the change in height from a break in a monolayer on the surface. The black triangle to the left of the color code indicates the zero plane. To obtain this micrograph, we use a silicon nitride probe with a resonant frequency of approximately 1.6 MHz and a nominal tip radius of 5 nm, and we operate the atomic force microscope with a scan resolution of 2 nm and a scan rate of 1.0 Hz. Nine measurements of two breaks in the same monolayer give a change in height of 0.340 nm $\pm$ 0.006 nm. This value of uncertainty denotes a confidence interval of 95% for a t–distribution with 8 degrees of freedom. The experimental and nominal values of the monolayer thickness agree within measurement uncertainty, indicating the accuracy of this calibration. The relative uncertainty of 1.8% of this calibration measurement of a subnanometer reference material nearly quadruples that of the calibration measurement of a submicrometer reference material in the paper. However, the absolute value of this uncertainty of 0.006 nm is an order of magnitude smaller than additional absolute uncertainties from roughness variation and flatness errors, and is therefore insignificant.

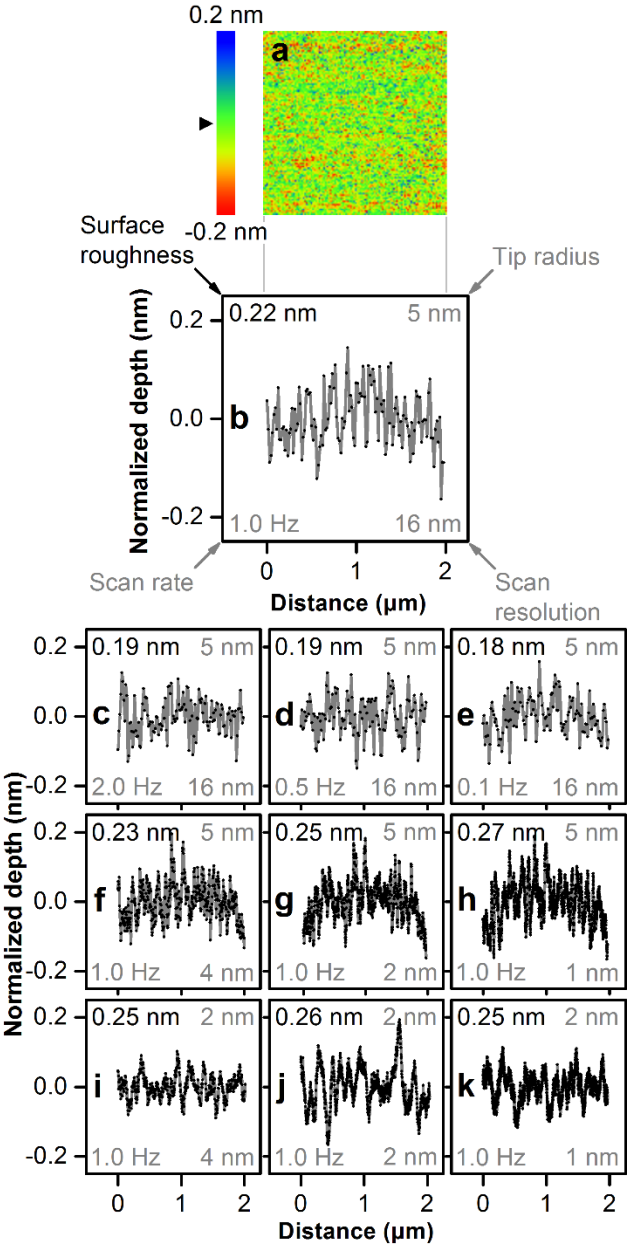

Fig. S2 Roughness uncertainty. (a) Atomic force micrograph and (b) corresponding section showing a milled silicon (100) surface with a planar topography that we measure using typical parameters. The black triangle to the left of the color code indicates the zero plane. (c-e) Sections of atomic force micrographs showing that the surface roughness that we measure fluctuates randomly as scan rate decreases. (f-h) Sections of atomic force micrographs showing that the roughness that we measure increases monotonically as scan resolution decreases, indicating a systematic bias from this parameter. (i-k) Sections of atomic force micrographs showing that the roughness that we measure remains constant as the radius of the probe tip decreases. We report surface roughness quantities as root-mean-square values from more than 6×10^2 data points with more than 4×10^4 replicate taps per data point. The measurement area of the test surface is 4 μm^2. Ignoring any correlations of these parameters, these ten measurements of roughness result in a

mean of 0.23 nm and a standard deviation of 0.03 nm, while the typical measurement parameters from the paper result in a roughness of 0.22 nm. Following the standard guidelines,[2] an evaluation of uncertainty by statistical means gives an uncertainty of 0.07 nm, representing a confidence interval of 95% for a t–distribution with 9 degrees of freedom. However, due to the systematic variation of the measurement results, an evaluation of the uncertainty by other means is also appropriate, in which case an uncertainty of 0.07 nm represents a confidence interval of 100% for a uniform distribution, or a conservative estimate of the limit of uncertainty. The low scatter of the roughness values in Fig. 3 relative to 0.07 nm suggests that our uncertainty evaluation is ultimately conservative.

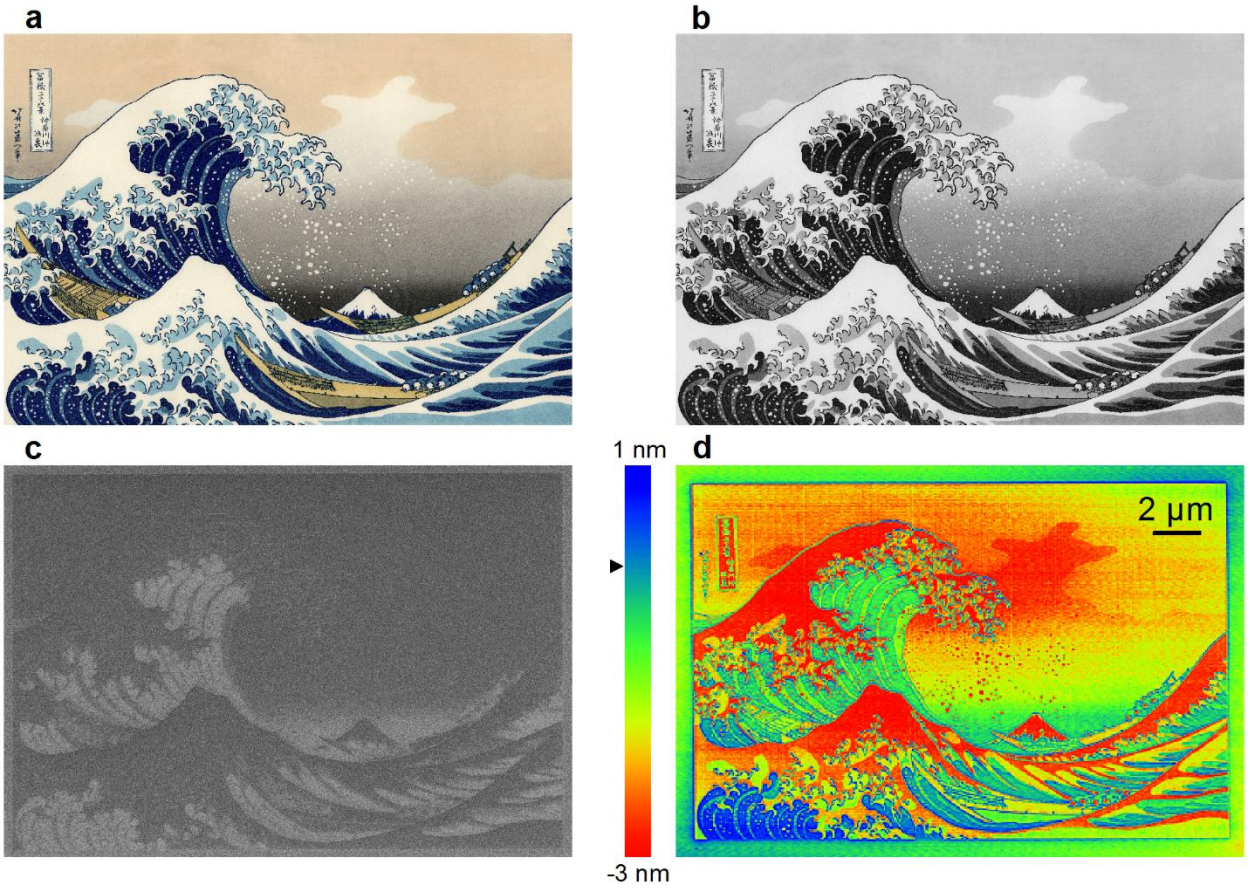

Fig. S3 Rapid prototyping. (a) Color bitmap image showing "Under a Wave off Kanagawa," published by Katsushika Hokusai between 1829 and 1833. We download this image, which is in the public domain, from the Internet. (b) Grayscale bitmap image after conversion from color to avoid artifacts from control of the dwell time by the blue value. We upload the grayscale image into our focused ion beam system, and mill the pattern into a silicon substrate in less than 10 s. (c) Scanning electron micrograph showing the resulting surface pattern. (d) Atomic force micrograph showing the surface pattern with a vertical range of 4 nm. The lateral resolution of the original pattern decreases in two stages through focused ion beam milling and atomic force microscopy. The ability to use bitmap images to directly pattern complex surfaces facilitates rapid prototyping. The black triangle to the left of the color code indicates the zero plane.

Table S1 Patterning variables

Fig.	Dose[a] (pC μm^{-2})	Ion current (pC s^{-1})	Dwell time per pixel* (μs)	Number of pixels	Number of passes	Pattern area (μm^2)
1b	8.9×10^{0}	1.6×10^{1}	1	1.6×10^{7}	200	5.7×10^{3}
2	$< 2.0\times10^{-2}$	4.0×10^{1}	[b]	1.2×10^{7}	1	1.2×10^{3}
2	$> 2.0\times10^{-2}$	9.0×10^{1}	1	1.2×10^{7}	[c]	1.2×10^{3}
3, S8, S9	3.0×10^{2}	1.2×10^{2}	1	1.5×10^{7}	105[d]	6.3×10^{2}
4	3.8×10^{2}	4.0×10^{1}	1	1.5×10^{7}	600[e]	9.7×10^{2}
5 (base)	2.2×10^{2}	4.4×10^{2}	1	1.4×10^{7}	350	9.8×10^{3}
5 (steps)	2.3×10^{2}	4.4×10^{2}	1	1.4×10^{7}	375	9.8×10^{3}
5 (inlet)	4.0×10^{2}	4.4×10^{2}	1	2.5×10^{6}	650	1.8×10^{3}
5 (outlet)	2.4×10^{2}	4.4×10^{2}	1	2.5×10^{6}	385	1.8×10^{3}
S2	8.6×10^{1}	1.2×10^{2}	1	1.5×10^{7}	30	6.3×10^{2}
S3c	2.7×10^{0}	1.6×10^{1}	1	1.6×10^{7}	60	5.7×10^{3}
S4	7.9×10^{-1}	9.4×10^{3}	1	9.0×10^{4}	[f]	[f]
S5	3.1×10^{-1}	9.4×10^{1}	1	1.2×10^{7}	335	1.2×10^{3}
S6a	1.7×10^{2}	1.9×10^{0}	1	2.0×10^{6}	600	1.4×10^{1}
S6b	5.4×10^{1}	1.9×10^{0}	1	2.6×10^{6}	100	9.0×10^{0}
S7	9.0×10^{1}	2.1×10^{2}	1	1.5×10^{7}	45	1.6×10^{3}
S10a	5.5×10^{1}	8.1×10^{2}	1	1.6×10^{7}	25	5.7×10^{3}
S10b	1.2×10^{3}	8.1×10^{2}	1	1.6×10^{7}	550	5.7×10^{3}
S10c	4.9×10^{1}	1.5×10^{2}	1	1.6×10^{7}	135	6.4×10^{3}
S10d	7.3×10^{2}	3.8×10^{2}	1	1.6×10^{7}	700	5.7×10^{3}
S11 (base)	1.2×10^{2}	4.5×10^{2}	1	1.4×10^{7}	185	9.8×10^{3}
S11 (steps)	1.1×10^{2}	4.5×10^{2}	1	1.4×10^{7}	165	9.8×10^{3}
S11 (inlet)	2.1×10^{2}	4.5×10^{2}	1	2.5×10^{6}	325	1.8×10^{3}
S11 (outlet)	1.8×10^{2}	4.5×10^{2}	1	2.5×10^{6}	275	1.8×10^{3}

[a] This column reports the maximum dose at a maximum dwell time of 1 μs per pixel, corresponding to a bitmap pixel with a white grayscale. Decreasing the dwell time from 1 μs per pixel to 25 ns per pixel delivers smaller doses, corresponding to bitmap pixels with darker grayscales.

[b] The dwell times are 25 ns, 100 ns, and 1 μs.

[c] The number of passes varies from 1 to 1600.

[d] The maximum dose corresponds to 105 passes. The number of passes varies from 15 to 105.

[e] The maximum dose corresponds to 600 passes. The number of passes varies from 210 to 600.

[f] The number of passes varies from 5000 to 50 and the pattern area varies from 5.3×10^{3} μm^2 to 5.3×10^{1} μm^2 to maintain a constant dose for the six data points in Fig. S4.

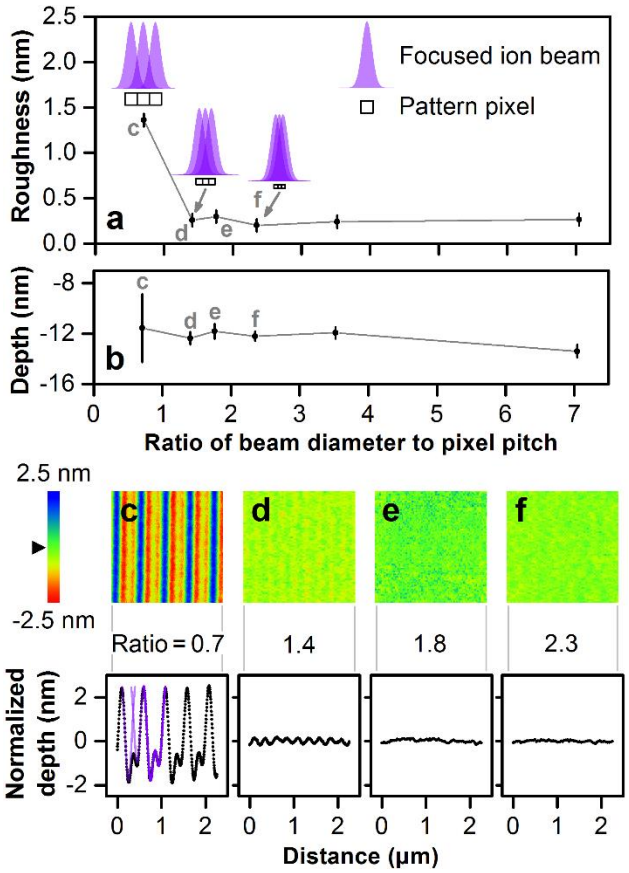

Fig. S4 Beam overlapping. The material is silicon (100). (a) Plot showing surface roughness, a coarse metric of surface topography, decreasing as the ratio of the diameter of the focused ion beam to the pitch of the pattern pixels increases to 1.5, overlapping the focused ion beam. In this test, the diameter of the focused ion beam remains constant while the pitch of the pattern pixels decreases. Vertical bars are confidence intervals of 95%. (b) Plot showing milled depth remaining nearly constant as overlap ratio increases. We maintain a nearly constant dose by decreasing both the pattern area and the number of passes. Vertical bars are two standard deviations of surface roughness, including the effects of nonplanar surface topography. (c-f) Atomic force micrographs and corresponding sections showing, in a finer analysis of surface topography, the transition from periodic nanostructures to planar surfaces. We normalize the section depths to zero at the mean values for clarity. The raster scanning of the focused ion beam forms lines in the case of inadequate overlapping of the beam profile. In this test, we estimate the beam diameter by fitting overlapping Gaussian functions to the peaks in the section of (c), using the method of damped least squares, resulting in an adjusted R^2 of 0.998 and a full-width at half-maximum of 172 nm ± 12 nm. The first two peaks in the section of (c) show this analysis in brief. At short dwell times, delays from the time of flight of ions may cause a scanning offset that produces the complex raster pattern. While we intend to pattern planar surfaces with subnanometer roughness, variable overlapping of the focused ion beam also enables control of the transition from periodic nanostructures to planar surfaces, which may be useful in the future. The black triangle to the left of the color code indicates the zero plane.

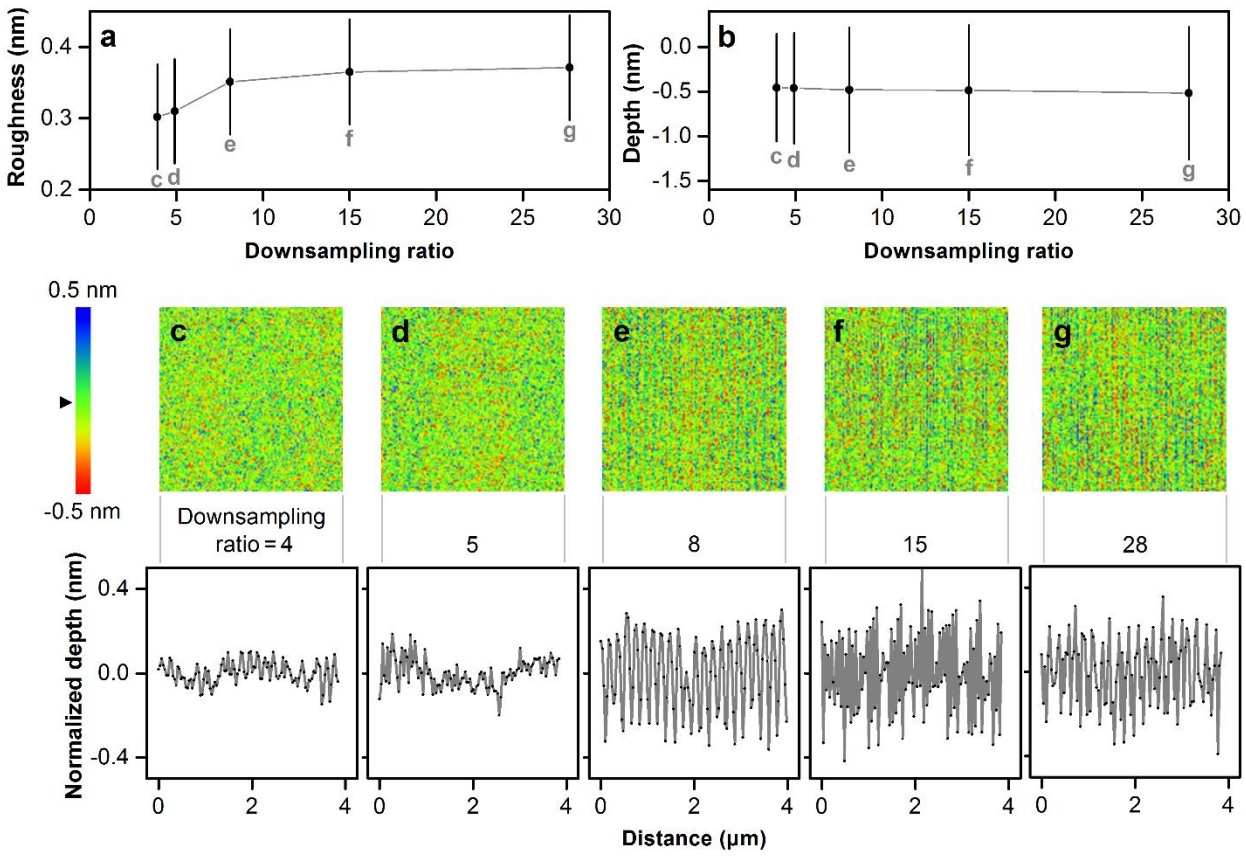

Fig. S5 Aliasing artifact. The material is silicon (100). If the number of pixels in a bitmap image exceeds the resolution of the display of our focused ion beam system, then the system computer downsamples the bitmap image, the pixel pitch becomes effectively larger in comparison to the focused ion beam, and an aliasing artifact occurs. Decreasing the magnification of the focused ion beam system induces this artifact. (a) Plot showing surface roughness, a coarse metric of surface topography, increasing with downsampling ratio. Vertical bars are confidence intervals of 95%. (b) Plot showing milled depth remaining nearly constant as downsampling ratio increases. Vertical bars are two standard deviations of surface roughness, including the effects of nonplanar surface topography. (c-g) Atomic force micrographs and corresponding sections showing, in a finer analysis of surface topography, the transition from planar surfaces with subnanometer roughness to periodic nanostructures with subnanometer crests and troughs. We normalize the section depths to zero at the mean values for clarity. The surface roughness is two-dimensional, while the sections emphasize one-dimensional aliasing errors. These results show that, for a particular focused ion beam profile, the magnification of the focused ion beam system can affect surface topography at the atomic scale. We report this artifact here for completeness but otherwise we avoid it. The black triangle to the left of the color code indicates the zero plane.

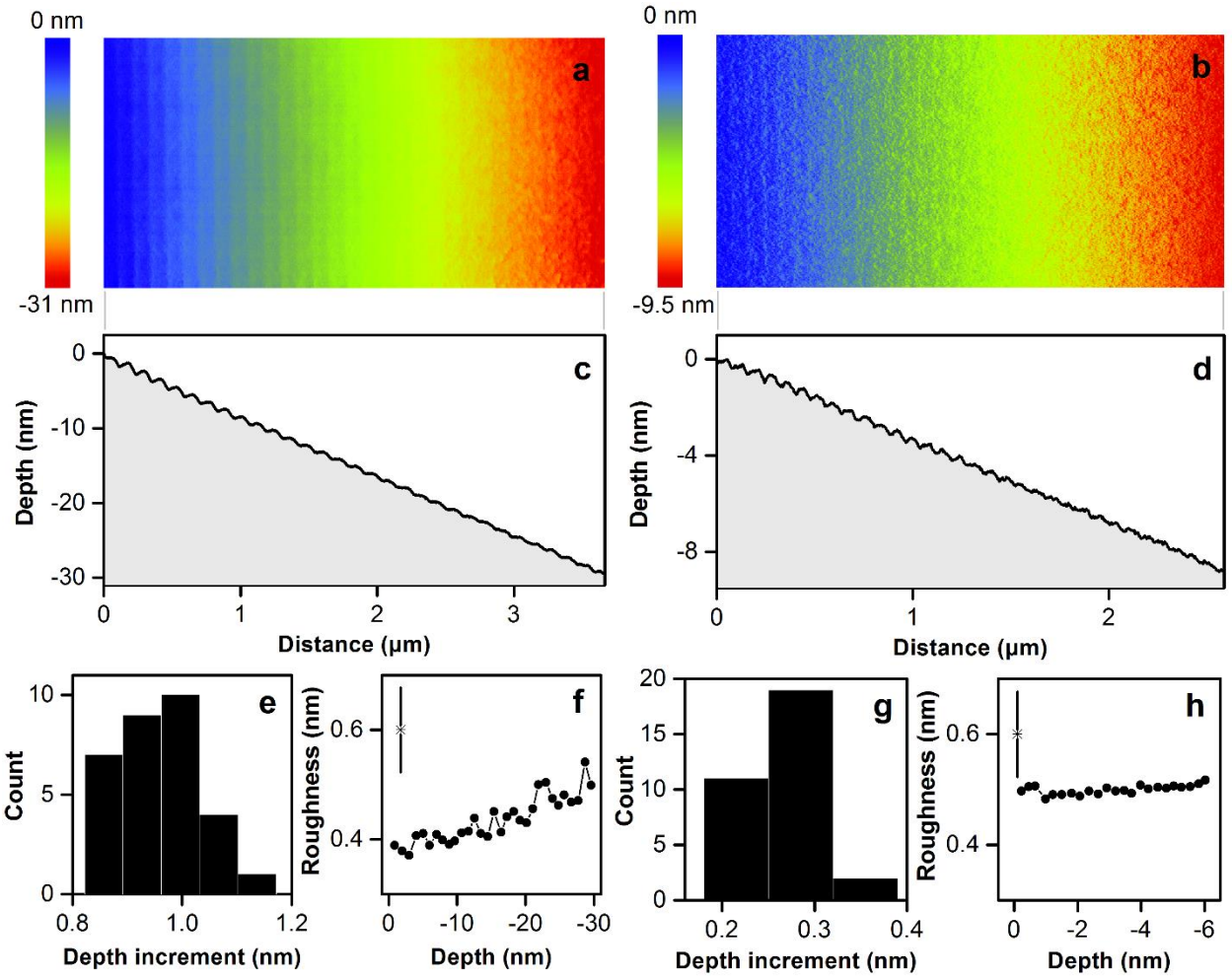

Fig. S6 Lateral resolution. (a and b) Atomic force micrographs and (c and d) corresponding sections showing staircase structures milled into silicon (100) with step widths of approximately 120 nm and approximately 80 nm, respectively. We treat the step edge roughness of a few tens of nanometers as a rough estimate of our lateral resolution. (e and g) Histograms showing subnanometer variation of depth increment as a measure of dimensional control. (f and h) Plots showing surface roughness, another measure of dimensional control, varying from 0.4 nm to 0.5 nm. Lone data markers in the upper left corners of (f and h) show representative values of uncertainty. The vertical dimensional control of these structures is comparable if not identical to that of Fig. 3c and Fig. 3d, showing that it is possible to simultaneously achieve vertical resolution of less than 1 nm and lateral resolution of less than 100 nm.

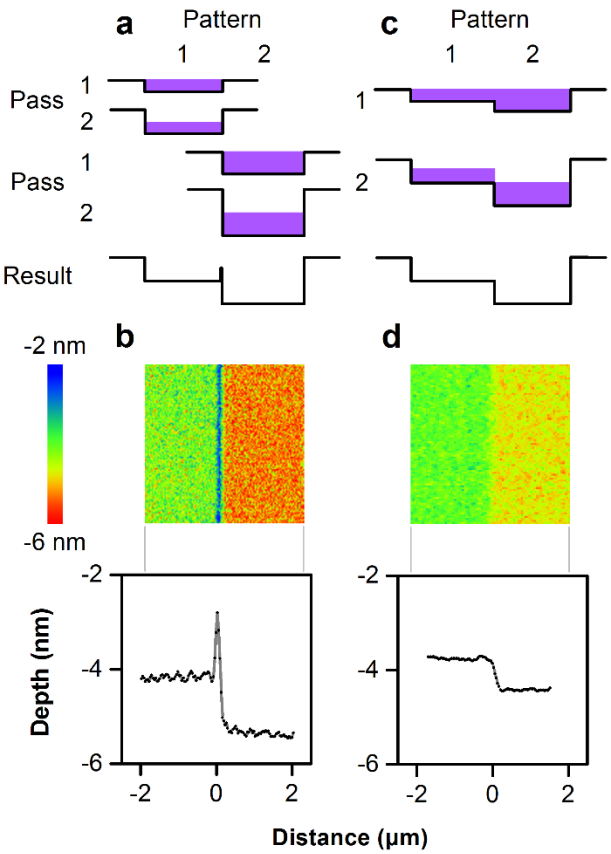

Fig. S7 Pattern integration. (a) Schematic showing the interface between two bitmap image patterns when all passes of each pattern are sequential, writing the patterns in series and forming an asperity. (b) Corresponding atomic force micrograph and section showing an interfacial asperity. (c) Schematic showing the interface between two bitmap image patterns when each pass of all patterns is sequential, writing the patterns in parallel and forming a smooth interface. (d) Corresponding atomic force micrograph and section showing a smooth interface.

Table S2 Ion penetration

Depth	Si	Si_3N_4	SiO_2
Mean	28 nm	19 nm	26 nm
Standard deviation	10 nm	6 nm	9 nm

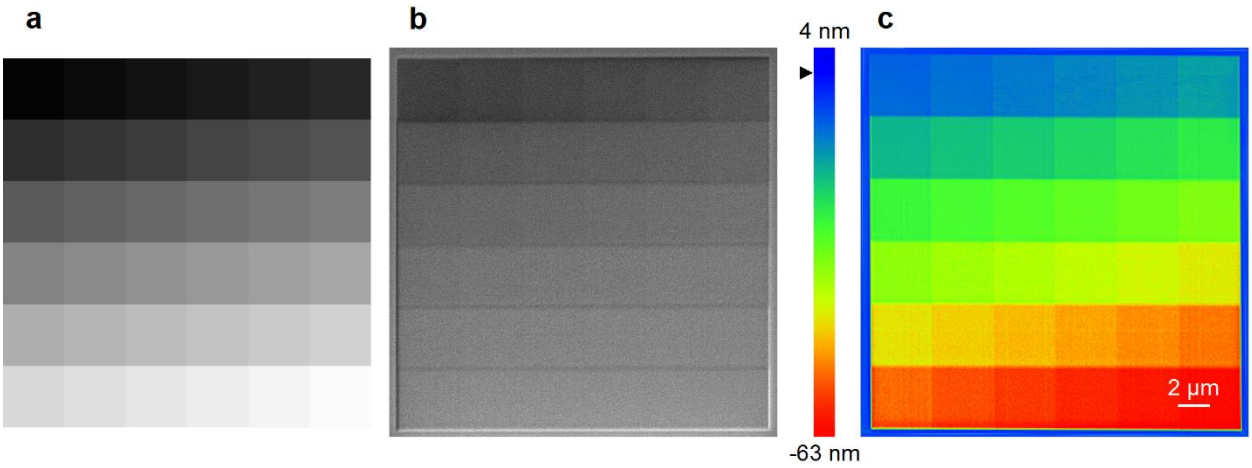

Fig. S8 Test pattern. (a) Grayscale bitmap image showing our test pattern, consisting of a 6 × 6 array of squares with 8-bit grayscale values varied from 1 for black to 255 for white. These values control the dwell time of the focused ion beam, from 25 ns per pixel to 1 µs per pixel. For silicon, seven iterations of this test pattern, with the number of passes of the focused ion beam increasing from 15 to 105, in increments of 15, result in as many test structures. (b) Scanning electron micrograph showing the deepest test structure that we mill into silicon. (c) Atomic force micrograph showing the same test structure with a color code for depth. The black triangle to the left of the color code indicates the zero plane. This test structure corresponds to the deepest data that Fig. 3 and S9 present (red rightward facing triangles). To reduce lateral flatness errors from atomic force microscopy, we first analyze each row of such test patterns independently, defining a local zero plane for each row by leveling two regions of approximately 3 µm × 4 µm on both sides. We then measure the depth of the central region of 2 µm × 2 µm of each square in each row in reference to the shallower proximate plane in a stepwise analysis.

Table S3 Fig. 3 analysis.*

Linear fit adjusted R^2	0.9989	0.9992	0.9992	0.9991	0.9991	0.9980	0.9982
Quadratic fit adjusted R^2	0.9991	0.9998	0.9999	0.9999	0.9998	1.0000	1.0000
Depth increment (nm)	0.17 ± 0.07	0.35 ± 0.08	0.57 ± 0.12	0.81 ± 0.14	1.05 ± 0.24	1.30 ± 0.29	1.56 ± 0.40
Dose increment (pC μm^{-2})	1.18	2.36	3.53	4.71	5.89	7.07	8.25

* We use the method of damped least squares to fit linear and quadratic models to the data in Fig. 3b. Depth increments are mean values ± two standard deviations, quantifying the distribution widths in Fig. 3c.

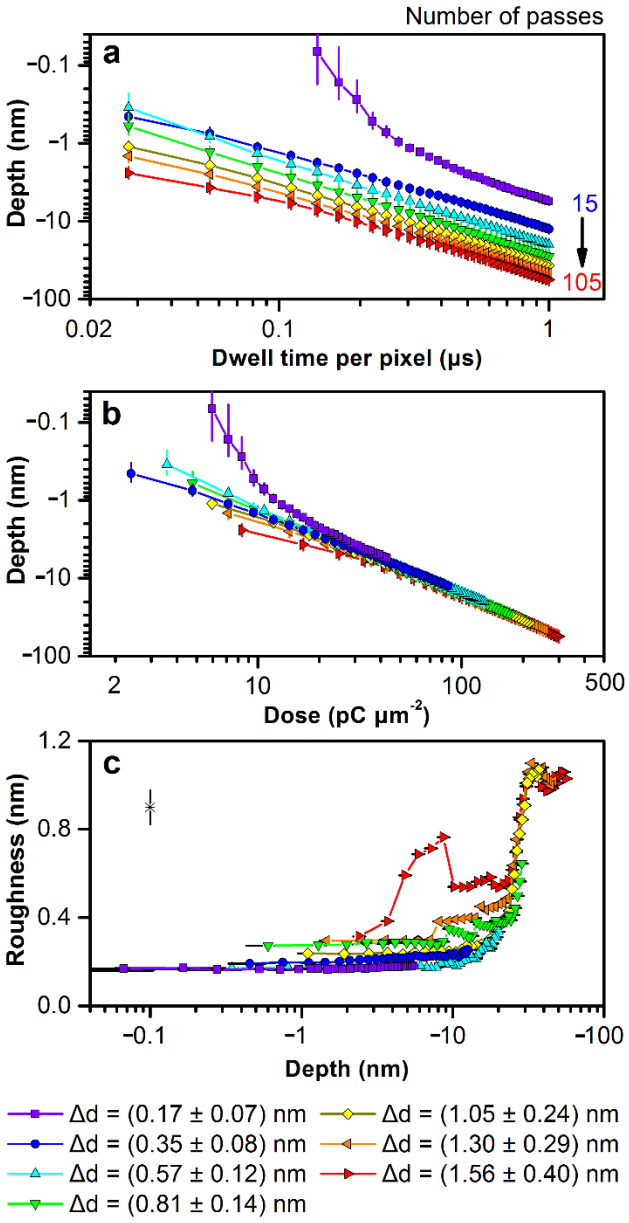

Fig. S9 Milling silicon. We replot the data from Fig. 3a, 3b, and 3d on logarithmic and linear-logarithmic scales. The logarithmic scale in depth cuts off data above the zero plane in Fig. S9a. (a) Plot showing milled depth below the zero plane increasing with dwell time and number of passes, which we color code. Vertical bars are confidence intervals of 95%. (b) Plot showing milled depth below the zero plane increasing with dose. The initial response depends on the dose rate, as the inset of Fig. 3b show. Vertical bars are confidence intervals of 95%. (c) Plot showing surface roughness increasing from approximately 0.2 nm for the smallest vertical features to a maximum of approximately 1.1 nm at a depth of approximately 60 nm below the zero plane. A lone data marker in the upper left corner of the plots shows a representative value of uncertainty.

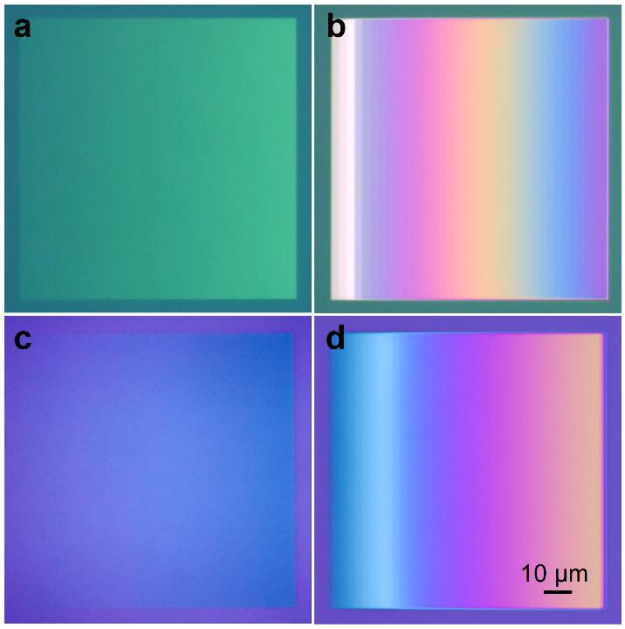

Fig. S10 Structural colors. Complex structures in dielectric films have depth profiles similar to those in Fig. 4a and b, resulting from 36 increments of dose increasing linearly from left to right. (a and b) Brightfield micrographs showing complex structures in a film of stoichiometric silicon nitride with a thickness of 392 nm ± 4 nm. The structures have maximum depths below the zero plane of (a) approximately 2.6 nm with a roughness of 0.19 nm ± 0.07 nm and (b) approximately 183 nm with a roughness of 0.37 nm ± 0.07 nm. (c and d) Brightfield micrographs showing complex structures in a film of silicon dioxide with a thickness of 507 nm ± 2 nm. The structures have maximum depths below the zero plane of (c) approximately 2.7 nm with a roughness of 0.31 nm ± 0.07 nm and (d) approximately 120 nm with a roughness of 1.76 nm ± 0.08 nm. Structural colors indicate changes in film thickness at the subnanometer scale and are in qualitative agreement with simulations of optical interference.[3]

Video S1 Nanoparticle separation. A video shows a time series of fluorescence micrographs at intervals of 5 min. Each fluorescence micrograph results in an exposure time of approximately 2 s with an acquisition time of 100 ms. The fluorescence micrograph in Fig. 5b, corresponding to the final fluorescence micrograph in the time series, has an acquisition time of 2.5 s.

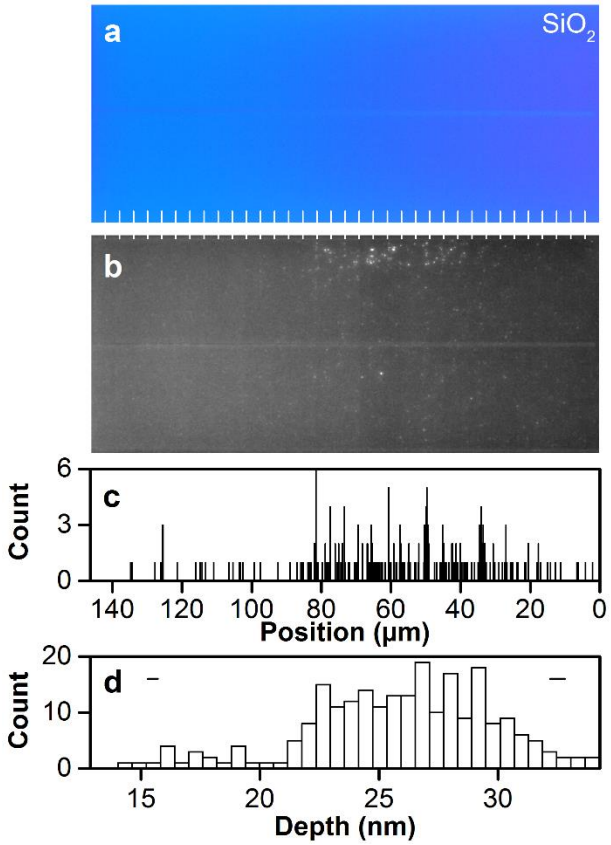

Fig. S11 Analytical separation. (a) Brightfield micrograph showing a staircase structure in silicon dioxide with 36 steps in milled depth from 14.2 nm ± 0.2 nm to 35.0 nm ± 0.3 nm below the zero plane. The horizontal feature in the center of the micrograph is a support structure with a width of approximately 650 nm that prevents potential collapse of the device during bonding. The colors correspond to Fig. 4f. (b) Fluorescence micrograph showing the size separation of nanoparticles in the resulting nanofluidic staircase. The nanoparticles have a mean diameter of 24 nm and a standard deviation of 3 nm, and reach positions of size exclusion at steps that become shallower than the diameters. Surface roughness reduces milled depths by 1.0 nm to excluded depths. (c) Histogram showing nanoparticle positions of size exclusion. Position uncertainties are negligible at the scale of this plot. Reference of nanoparticle position to excluded depth places nanoparticles into bins with sizes of the depth increment or separation resolution of 0.6 nm. (d) Histogram showing corresponding excluded depths. Two horizontal bars show representative confidence intervals of 95% corresponding to minimum and maximum values of dimensional uncertainty across the nanofluidic staircase. Statistical analysis of this histogram gives the size distribution with a mean of 25.5 nm ± 3.2 nm and a standard deviation of 4.0 nm ± 0.5 nm, validating the result. The latter uncertainties are sampling errors.

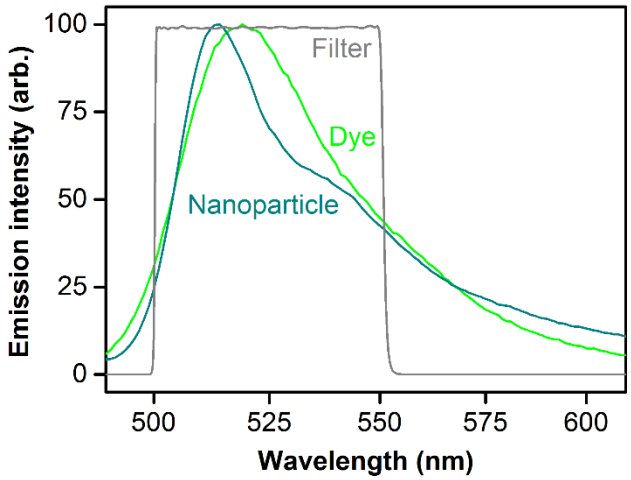

Fig. S12 Emission spectra. Plot showing manufacturer data of the emission spectra for the dye that we use to calibrate optical interference and the nanoparticles that we test, as well as the bandpass of the emission filter. The emission spectra of dye and nanoparticles are similar and we neglect the small discrepancy between them. We note that even if we ignore the effects of optical interference and do not perform this calibration, then the scaling exponent *b* in the paper changes only from 4.0 to 3.8, although the systematic effects in Fig. 6b become evident as systematic errors in Fig. 6c, worsening the fits and impeding a quantitative analysis. This is because the dye calibration data in Fig. 6b deviates systematically but not grossly from a linear trend over the range of nanoparticle test data in Fig. 6c. Therefore, our conclusion about nonvolumetric scaling is robust against the effects of optical interference.

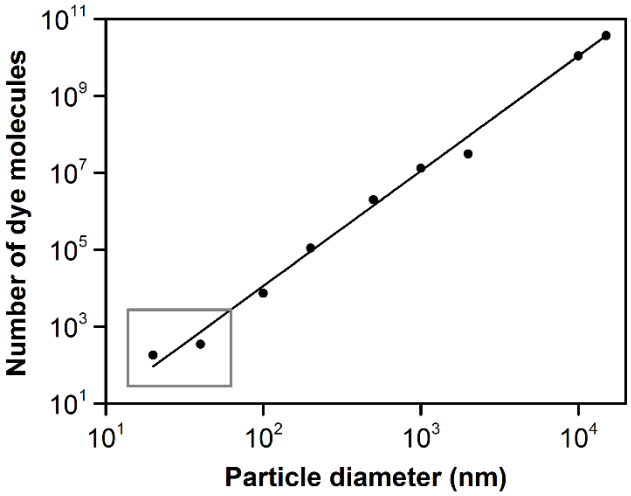

Fig. S13 Dye loading. Plot showing manufacturer data of the number of dye molecules in particles with diameters that range from 20 nm to 20 µm. We fit the model $N_{dye} = aD^b$, where N_{dye} is the number of dye molecules, D is the particle diameter, and a and b are floating constants, to the data using the method of damped least squares. This gives a value of b of 2.99 ± 0.01, indicating that the number of dye molecules scales with particle volume over the full range of particle diameters. This analysis is only semi-quantitative, however, as the manufacturer does not report

measurement uncertainties, scatter of the data is evident, and the density of data is too low to quantify the relationship between nanoparticle size and fluorescence intensity for diameters in the range of our experiment. In contrast, we present data in Fig. 6b with quantitative uncertainties and with a density that is an order of magnitude higher, by fractionating a size distribution that comprises one data point in the gray inset.

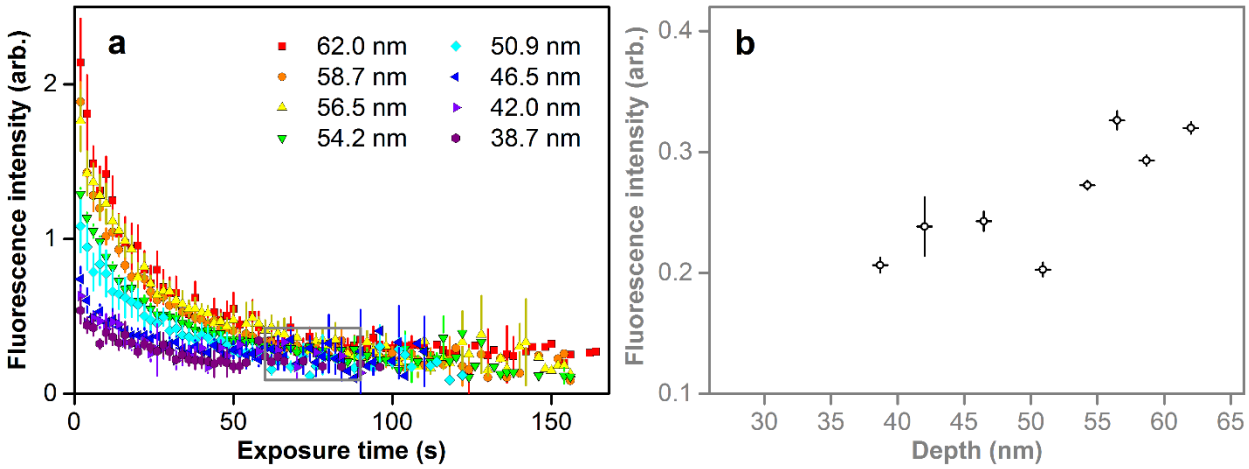

Fig. S14 Photobleaching analysis. (a) Plot showing the decreasing fluorescence intensity of nanoparticles of different diameters with increasing exposure time, indicating that the boron dipyrromethene dye molecules in the polystyrene nanoparticles are photobleaching. After an exposure time of approximately 60 s, the fluorescence intensities decay to terminal values. (b) Inset plot showing terminal values of fluorescence intensity. These values increase only slightly with excluded depth, corresponding to nanoparticle diameter, and scatter of the data beyond measurement uncertainty is evident. This result is inconsistent with volumetric autofluorescence of polystyrene, indicating the possible presence of faintly fluorescent inner volumes of approximately constant diameter. Vertical bars are confidence intervals of 95%. Horizontal bars are limits of uncertainty, corresponding to the depth increment.

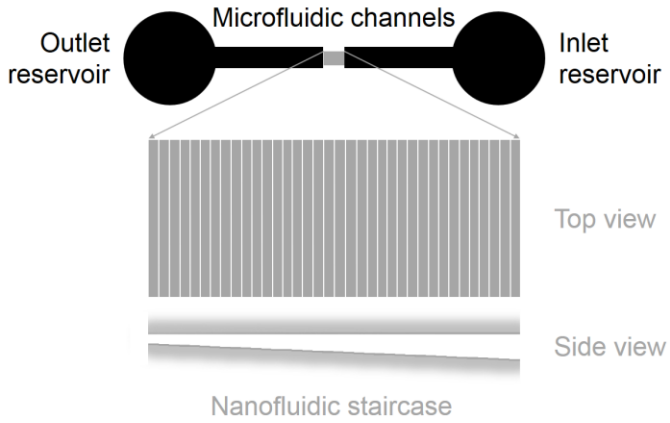

Fig. S15 Device layout. Schematic showing the overall layout of the device.

Note S1 Interference calibration

We express our calibration process in equation notation. For clarity of notation, we use an index of step number here in the supplement, rather than a value of nanofluidic depth or excluded depth as in the paper.

$$I_{\mathrm{dye,cal_n}} = \frac{I_{\mathrm{dye_n}} - I_{\mathrm{bg_n}}}{\frac{I_{\mathrm{ff_n}}}{I_{\mathrm{ff_{36}}}}}$$

n: Step number from 1 to 36
$I_{\mathrm{dye,cal_n}}$: Fluorescence intensity of dye after calibration (arbitrary units [arb.])
$I_{\mathrm{dye_n}}$: Emission intensity of dye before calibration (analog-to-digital units [ADU])
$I_{\mathrm{bg_n}}$: Emission intensity of corresponding background before calibration (ADU)
$I_{\mathrm{ff_n}}$: Fluorescence intensity of dye after flatfield correction (arb.)
$I_{\mathrm{ff_{36}}}$: Maximum fluorescence intensity of dye on step 36 after flatfield correction (arb.)

$$I_{\mathrm{F}} = I_{\mathrm{np,cal_n}} = \frac{\langle I_{\mathrm{np}} - I_{\mathrm{np,bg}} \rangle_{\mathrm{n}}}{\frac{I_{\mathrm{ff_n}}}{I_{\mathrm{ff_{36}}}}} \times \frac{\frac{\delta_{\mathrm{n}}}{\delta_{36}}}{\frac{I_{\mathrm{dye,cal_n}}}{I_{\mathrm{dye,cal_{36}}}}}$$

$I_{\mathrm{F}} = I_{\mathrm{np,cal_n}}$: Fluorescence intensity of nanoparticles after calibration (arb.)
I_{np}: Emission intensity of single nanoparticles before calibration (ADU)
$I_{\mathrm{np,bg}}$: Emission intensity of local background before calibration (ADU)
δ_{n}: Nanofluidic depth
δ_{36}: Maximum nanofluidic depth of step 36
$I_{\mathrm{dye,cal_{36}}}$: Maximum fluorescence intensity of dye on step 36 after calibration (arb.)

We implement this calibration process involving dye over the 36 steps of the staircase structure, as Fig. 5 and 6 show. However, due to the small numbers of nanoparticles that we sample at the tails of the size distribution, we show only 28 values of fluorescence intensity for nanoparticles.

Supplementary references

1 M. Le Guillou, J. N. Rouzaud, D. Deldicque, N. Toulhoat, Y. Pipon and N. Moncoffre, *Carbon*, 2015, **94**, 277-284.
2 B. N. Taylor and C. E. Kuyatt, *Guidelines for Evaluating and Expressing the Uncertainty of NIST Measurement Results.* 1994 ed.; National Institute of Standards and Technology, Technical Note 1297: 1994; pp 1-24.
3 J. Henrie, S. Kellis, S. M. Schultz and A. Hawkins, *Opt. Express*, 2004, **12**, 1464-1469.